Anais da Academia Brasileira de Ciências (2007) 79(1): 17–28
(Annals of the Brazilian Academy of Sciences)
ISSN 0001-3765
www.scielo.br/aabc

New tools to study biophysical properties of single molecules and single cells

MÁRCIO S. ROCHA and OSCAR N. MESQUITA

Universidade Federal de Minas Gerais, Departamento de Física, ICEx, Av. Antônio Carlos, 6627
Caixa Postal 702, 30123-970 Belo Horizonte, MG, Brasil

Manuscript received on February 2, 2006; accepted for publication on September 9, 2006;
presented by LUIZ DAVIDOVICH

ABSTRACT

We present a review on two new tools to study biophysical properties of single molecules and single cells. A laser incident through a high numerical aperture microscope objective can trap small dielectric particles near the focus. This arrangement is named optical tweezers. This technique has the advantage to permit manipulation of a single individual object. We use optical tweezers to measure the entropic elasticity of a single DNA molecule and its interaction with the drug Psoralen. Optical tweezers are also used to hold a kidney cell MDCK away from the substrate to allow precise volume measurements of this single cell during an osmotic shock. This procedure allows us to obtain information about membrane water permeability and regulatory volume increase. Defocusing microscopy is a recent technique invented in our laboratory, which allows the observation of transparent objects, by simply defocusing the microscope in a controlled way. Our physical model of a defocused microscope shows that the image contrast observed in this case is proportional to the defocus distance and to the curvature of the transparent object. Defocusing microscopy is very useful to study motility and mechanical properties of cells. We show here the application of defocusing microscopy to measurements of macrophage surface fluctuations and their influence on phagocytosis.

Key words: optical tweezers, defocusing microscopy, single molecules, macrophages, water transport, cell motility.

INTRODUCTION

Physics can contribute to understand biological phenomena in many ways. One of the ways is by developing new quantitative tools to investigate biological phenomena. In this article we will describe the use of two recently developed techniques: optical tweezers and defocusing microscopy. Optical tweezers were invented in the 70s by A. Ashkin (Ashkin 1970) and have become an important tool to manipulate single biological molecules like DNA and single cells. It can exert forces in the pico Newton range being appropriate to perform elasticity measurements in single molecules and single cells, measurements of stall forces of molecular motors, among other applications (Ashkin and Dziedzic 1987, Ashkin 1992, Svoboda and Block 1994, Grier 2003). Here we will show the use of optical tweezers both as a force sensor to measure DNA and DNA/drug elasticity and also as a micromanipulation tool to study osmotic transport through a single kidney cell. Defocusing microscopy is a new light microscopy technique invented in our laboratory that allows us to observe transparent objects (phase objects), like cytoskeleton and cell membranes, without requiring phase plates, polarizing prisms, etc., used in phase contrast and DIC microscopy techniques. While the image contrast in phase contrast microscopy is proportional to the phase object thickness and in DIC microscopy proportional to the thickness gradient, defocusing microscopy image contrast is proportional to the curvature of the observed phase object. Since curvature is the most important and energy costing deformation of cell surfaces, defocusing microscopy gives us a parameter (cell surface curvature) from which one can

Correspondence to: Oscar N. Mesquita
E-mail: mesquita@fisica.ufmg.br

directly assess cell motility. We use defocusing microscopy to measure surface fluctuations and ruffling activity of macrophages. With the combination of optical tweezers and defocusing microscopy we are able to control and promote single phagocytosis events and simultaneously measure phagocytosis time and motility of macrophages. We hope with these experiments to have a better understanding of the underlying mechanisms of cell motility and their relation to phagocytosis.

NEW TOOLS

Optical Tweezers

A single laser beam focused by a high numerical aperture objective is able to trap small dielectric particles near the lens focus. Such an arrangement is called optical tweezers (Ashkin 1970, 1992, Ashkin and Dziedzic 1987). The trapped particle is in a potential energy well, similar to a mass-spring system. To pull the particle away from the equilibrium position a force has to be applied on the particle. If one knows the tweezers spring constant (stiffness) and by measuring the displacement of the particle in relation to its equilibrium position, one can obtain the applied force, since the force is the product of the stiffness times the displacement. In general, in most practical cases, optical tweezers are able to exert forces in the picoNewton (10^{-12} N) range. Even though optical tweezers have been widely used during the last decade, only recently an exact theory has been put forward (Maia Neto and Nussenzveig 2000, Mazolli et al. 2003). We have developed, in our laboratory, a method based on dynamic light scattering for measuring both the tweezers stiffness and the displacement of particles in relation to their equilibrium position, with nanometer resolution (Viana et al. 2002). Therefore, optical tweezers can be used to manipulate small objects and to measure forces in the pN range. Later, we will show applications were both capabilities are used.

Defocusing Microscopy

Most biological samples of interest are nearly transparent to visible light. The standard light microscopy techniques to visualize such transparent objects (phase objects) are phase-contrast microscopy (PhC) and differential interference contrast microscopy (DIC), in addition to fluorescence techniques. Phase-contrast returns image contrast that is proportional to the phase difference, while DIC returns values proportional to the gradient of phase difference introduced by the phase object. While they are good techniques for visualization and for measuring transverse dimensions, other quantitative information is difficult to obtain from the images. In addition, the use of phase plates, filters and prisms makes these techniques more elaborate requiring a good expertise to work with them. We recently developed a new simple bright-field microscopy technique, which we believe is a break-through in this field, because it is easy to use and provides good quality quantitative data on cell motility. It is known that phase objects become visible in a slightly defocused bright-field light microscope (Fig. 1).

Fig. 1 – Stains on a microscope coverglass. a) For positive defocusing, b) in focus (object invisible) and c) for negative defocusing.

We have made a mathematical model for a defocused microscope and showed that the image contrast observed in this case is proportional to the defocus distance and to the curvature of the object, for objects with uniform index of refraction (Agero et al. 2003). In simple words, our mathematical model predicts that phase objects play the role of thin lenses that converge or diverge light depending on their curvatures, which causes light and dark contrast images that can be measured and quantitatively studied, with image processing techniques (Agero et al. 2003). In Fig. 2 we show a schematic drawing of a phase object, as well as the important variables to understand what we named by "defocusing microscopy" (DM).

Defocusing microscopy is very useful to study motility and mechanical properties of cells, since, in general, cells are in a state of zero surface tension, therefore the most energy costing fluctuations and dynamics are related to curvature deformations, the parameter directly measured with DM. The basic equation of DM is shown below,

$$\begin{aligned} C(x,y) &= \frac{I(x,y) - I_0}{I_0} \\ &= \Delta n\,[\Delta f - h(x,y)]\,\nabla^2 h(x,y), \end{aligned} \tag{1}$$

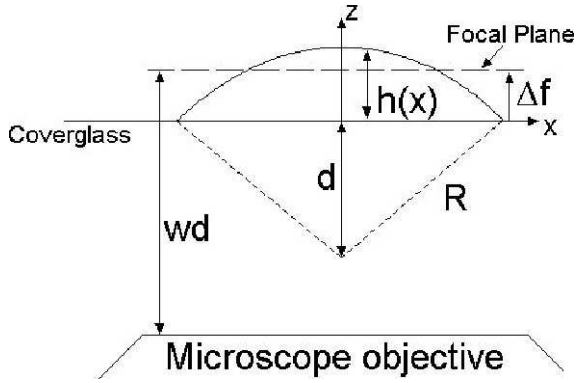

Fig. 2 – Schematic drawing of a cap-shaped phase object, as well as the important variables to understand the defocusing microscopy technique.

where $C(x, y)$ is image contrast, $I(x, y)$ is image intensity at the position (x, y), I_0 is the background image intensity out of the object, Δn is the difference in refractive index between the object and the medium, Δf is the defocus distance measured in relation to the coverslip where the object lies, $h(x, y)$ is the thickness profile of the phase object in relation to the coverslip, and $\nabla^2 h(x, y)$ is the 2D-Laplacian of the thickness profile which is equal to the local object curvature. In this expression we assume also that the microscope depth of focus is smaller than the object thickness. In our experiments, with an objective of numerical aperture equal to 1.4 the depth of focus is of the order of 0.3 μm.

We built artificial phase objects to test Eq. 1, which consisted of spherical caps made out of polystyrene. An example is shown in Fig. 3a, b.

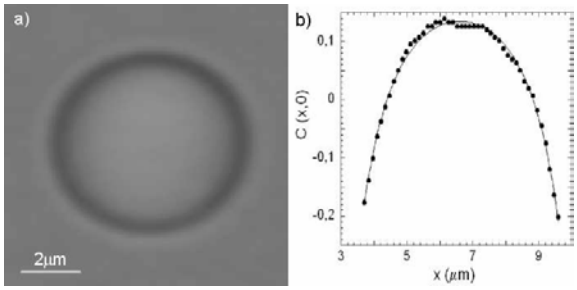

Fig. 3 – a) Image of a defocused spherical cap of polystyrene in air; b) contrast along the horizontal diameter fitted with Eq. 1; from the fit $R = 8.09 \pm 0.03 \mu m$, and Δn = 0.61 $\pm$ 0.02, resulting in a polystyrene refractive index equal to 1.61, which agrees with the table value.

In Fig. 3a it is displayed a spherical cap image observed under a defocused microscope. In Fig. 3b it is displayed the contrast profile along a diameter together with a theoretical fit using Eq. 1. The agreement is excellent and we can quantitatively determine the curvature radius of the spherical cap and its refractive index. The details of these tests and sample preparation can be found in our references (Agero et al. 2003, 2004). It is important to mention that the contrast profile in Fig. 3b has positive and negative values even though the object curvature does not change. It means that the focal plane of the microscope lies inside of the object as in the scheme showed in Fig. 2. For thin objects compared to the defocus distance ($\Delta f >> h(x, y)$), Eq. 1 can be simplified to read,

$$C(x, y) = \Delta f \Delta n \nabla^2 h(x, y). \qquad (2)$$

APPLICATIONS

Below we show some applications of the techniques described above, which have been carried out in our laboratory. All applications are made with the use of an inverted infinity corrected microscope from Nikon (Eclipse TE300), with a SDL (5422-H1) infrared laser for the optical tweezers and a He-Ne laser whose backscattered light by the trapped beads is the probe to measure bead displacement and Brownian motion. A scheme of our apparatus is shown in Fig. 4.

Entropic Elasticity of Single DNA Molecules and Single DNA Complexes

Optical tweezers have the great advantage to permit manipulation and observation of a single individual object, like a microsphere, a macromolecule or even a live cell.

In this section we study the entropic elasticity variation of a λ-DNA molecule in a solution with the photosensitive drug psoralen (*Furo 3,2-g Coumarin*, $C_{11}H_6O_3$) using optical tweezers and intensity autocorrelation spectroscopy. To do this, we attach a polystyrene microsphere of diameter 2.8μm to one end of the molecule. The other end of the molecule is then attached to a microscope coverslip, so we can manipulate and stretch the molecule using optical tweezers, which trap the polystyrene bead, to obtain a force versus extension curve. Displacements are measured by analyzing the backscattered light from the polystyrene bead attached

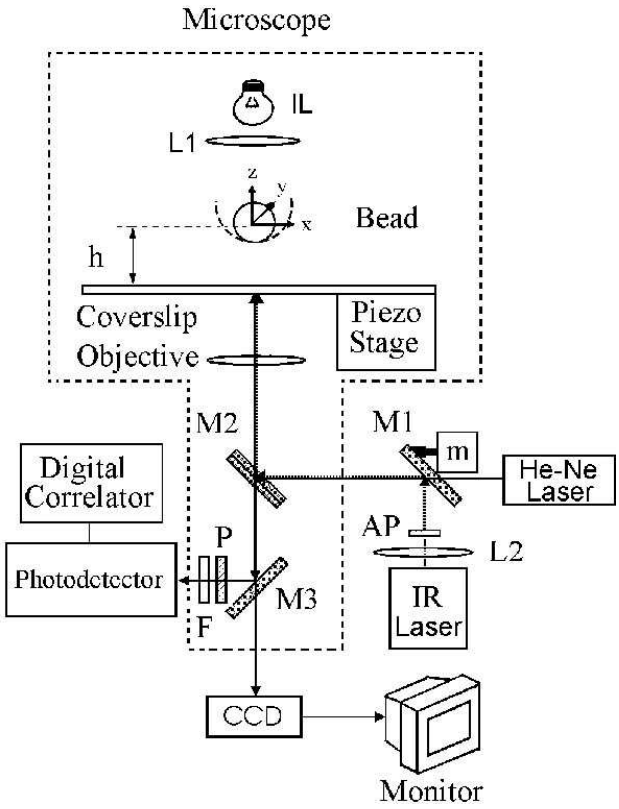

Fig. 4 – Experimental setup around the Nikon TE300. *AP* is an anamorphic prism, *M1* and *M2* are dicroic mirrors for maximizing IR reflections, *m* is a d.c. motor to move the IR beam, *M3* is a movable prism inside the microscope to switch different paths, *P* is a polarizer, *F* is a 632.8 nm line filter, the Photodetector is an EGG SPCM-200-PQ-F500, and the Digital Correlator is a Brookhaven BI-9000AT.

to the DNA molecule (Rocha et al. 2004). To do this, we use a He-Ne laser (λ = 632.8 nm) as the scattering probe, in addition to the trapping laser (λ = 832 nm).

Long molecules like DNA are very good polymers. One can use the impressive amount of knowledge accumulated along the years known as "Polymer Physics", to explain some of the physical properties of DNA and other biological molecules. Polymers in solution tend to become coiled due to collision with the molecules of the solution medium. The coiled equilibrium configuration is the one that maximizes entropy.

Therefore, an external force has to be applied to uncoil a polymer out from its equilibrium configuration. For small displacements the polymer behaves as a mass-spring system, such that the force applied is equal to the end-to-end distance multiplied by a constant, the entropic stiffness of the polymer. For larger displacements up to about the contour length of the polymer, the Marko-Siggia (Marko and Siggia 1995) approximate expression for the entropic force gives a reasonably good description of this effect, namely,

$$F = \frac{k_B T}{A}\left[\frac{z}{L} + \frac{1}{4\left(1-\frac{z}{L}\right)^2} - \frac{1}{4}\right], \qquad (3)$$

where F is the entropic force, k_B is Boltzmann constant, T is the absolute temperature, A is the persistence length of the polymer, L is the contour length of the polymer and z is the average end-to-end distance. The persistence length A gives a measure of the polymer flexibility, since it is the average distance between consecutive folded regions of the polymer. If A is of the order of L, the polymer does not have folded regions and behaves as a rigid rod. On the other hand, if A is much smaller than L the polymer is very flexible with many folded regions.

A curious result is that if a polymer is very flexible, with small persistence length, a larger force has to be applied to uncoil it as expressed by Eq. 3. As the end-to-end distance z approaches the contour length L, the value of F increases considerably. Naturally, the model is no longer valid for $z = L$ when the entropic force diverges. During the entropic regime there is no, or very little, stretching of chemical bonds of the polymer. In the limit where z approaches L, chemical bonds start to being stretched and the entropic model is no longer valid. Therefore, Eq. 3 is valid up to about $z = 0.95L$.

In our laboratory, using optical tweezers and videomicroscopy techniques we are able to stretch single DNA molecules and measure their persistence lengths. We also study the interaction between the photosensitive drug psoralen and DNA by measuring the change in persistence length of the complex formed when illuminated with UVA light. Psoralen is used in the treatment of some skin diseases with the technique named PUVA: Psoralen followed by UVA light (Coven et al. 1998, Tran et al. 2001). In order to measure the entropic elasticity of DNA and DNA+Psoralen, a polystyrene bead of diameter 2.8 μm is linked at one end of a DNA molecule, and the other end of the DNA is linked to the coverslip of the sample cell. The bead is trapped by the optical tweezers. As one moves the microscope stage, the DNA single molecule is stretched. The bead, originally at the equilibrium position in the trap, is also displaced from it. By measuring the displacement of the bead and knowing the stiffness of the tweezers one can then obtain the entropic force. The details of sample preparation, as well as the experimental procedure of these stretching experiments can be found in our references (Rocha et al. 2004, Viana et al. 2002). A typical result of a stretching experiment with a single DNA molecule of λ-phage is shown in Fig. 5.

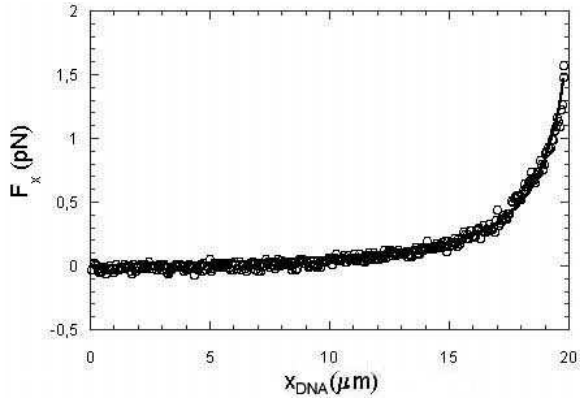

Fig. 5 – Force (x-component) as a function of elongation for a DNA molecule. Fitting this curve to Eq. 3, we determine the persistence length *A* and the contour length *L*.

Equilibrium Measurements

Typically, the persistence length for a single DNA molecule is of the order of 45 nm. When we add the drug psoralen, which intercalates the DNA, the persistence length increases to around 70 nm. When the complex is illuminated with UVA light (like in PUVA treatment for vitiligo and psoriasis), psoralen makes cross-links with opposite strands pyrimidines increasing the persistence length up to about 110 nm. After that, by illuminating the complex with UVB light, the crosslinks are broken, remaining only monoadducts, with a consequent decrease in persistence length, down to 35 nm. These results are shown in Table I. Therefore, this technique can be used to study drug-DNA interaction and protein-DNA interaction. Since we do not directly measure the actual light intensity on the sample, we wait enough time for the complex to achieve a constant persistence length for a given light intensity. For the intensity used in our experiments, we can perform the measurements after illuminating the sample for 30 minutes. The illuminating lamp is turned off during the measurements.

In Table I the results using different lights are displayed. These results and the details of sample preparation are described in our article ref. (Rocha et al. 2004). The drug concentration used in these experiments was C = 1.5μg/ml.

The UV light source used in our measurements is a Nikon LH-M100C-1. To illuminate the sample with only UVA or UVB wavelengths, we use bandpass filters.

Persistence Length Kinetics

Kinetics measurements of the persistence length are performed using the same DNA molecule. Without illuminating the sample, we first move the microsphere to an arbitrary position on the backscattering profile using a motor. Then, we turn on the UVA light and collect the backscattered light intensity by the microsphere. Since the UVA light activates DNA-psoralen linkage, we

TABLE I
Equilibrium measurements results for the persistence length of DNA and DNA-psoralen complexes.

Sample	Illumination	A (nm)
DNA	Any light (including UVA + UVB)	45 ± 5
DNA-Psoralen	Green light (λ = 500±20 nm)	64 ± 6
DNA-Psoralen	Blue light (λ = 450±20 nm)	67 ± 7
DNA-Psoralen	UVA light	107 ± 10
DNA-Psoralen	UVB light (after UVA)	34 ± 4

should see variation on the backscattered intensity as a function of time. This fact occurs because the rigidity of the sample is modified by the linkage, and consequently, the force exerted by the DNA on the microsphere varies, moving the microsphere along the backscattering profile. We then transform backscattered intensity into force, obtaining the force exerted by the DNA molecule as a function of time while the sample is illuminated. To obtain the persistence length as a function of time, we suppose that the contour length does not vary so much during the illumination, *i.e.*, we use a constant value of L, since the experiment is performed in the low-stretching regime (Rocha et al. 2004). Figure 6 is a typical result obtained with this procedure, showing how the persistence length varies on time when the sample is illuminated with UVA light.

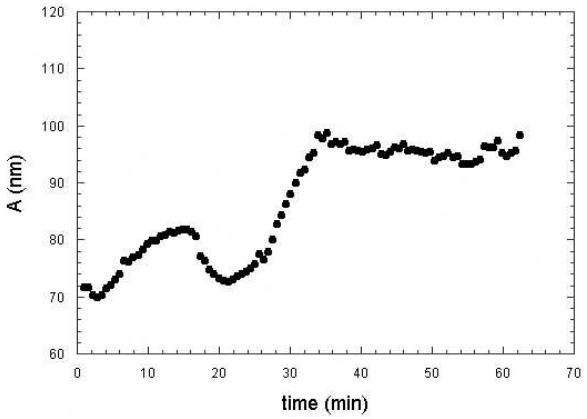

Fig. 6 – Persistence length as a function of time while illuminating the sample with UVA light.

Observe that the persistence length initially oscillates and then stabilizes at a value close to the reported in Table I after approximately 35 minutes. We do not understand yet the cause of such oscillations. Observe also that the initial value of the persistence length on Fig. 6 is close to those reported in lines 3 and 4 of Table I, which correspond to the intercalation situation.

Finally, we remember that the kinetics result showed in Fig. 6 corresponds to a unique DNA-psoralen complex, while the values reported in Table I refer to averages over many different molecules. The persistence length values of the particular DNA-psoralen complex showed in Fig. 6 agrees with Table I within 8%.

Water Transport Through a Single Kidney Cell

Pure lipid biological membranes are poorly permeable to water (10^{-5} to 10^{-4} cm/s), while water permeability of plasma membranes of epithelial cells involved in fluid transport can be much higher (10^{-3} to 10^{-1} cm/s) (Zeidel 1998). This observation led to the identification of a family of molecular water channels (aquaporins) that mediate and regulate water transport across plasma membranes (Agre 2000, Verkman and Mitra 2000). In order to determine whether water channels can account quantitatively for the water permeability observed in epithelial cell plasma membranes several model systems and different techniques have recently been developed to measure water permeability (Farinas et al. 1995, 1997, Timbs and Spring 1996, Zelenina and Brismar 2000, Maric et al. 2001). Water transport is ubiquitous in cells; therefore the technique described here is of general applicability in cell biology. In particular, precise measurements of water permeability in kidney cells are important as part of the understanding of renal disorders, hypertension, and how drugs can affect them. The central idea of most experiments is to submit layer of cells or tissues to an osmotic up or down shock and measure variation of cell

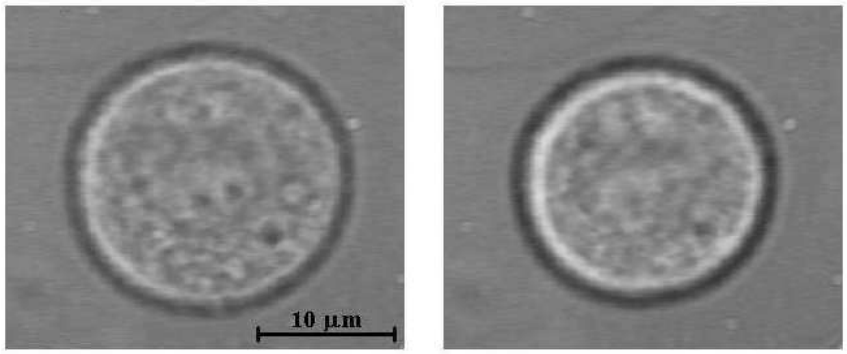

Fig. 7 – Left: Bright-field image of an optically trapped MDCK cell in equilibrium in a medium of 300 mOsm. Right: Image of the same cell 15s after a hyperosmotic shock of 200 mOsm.

volume as a function of time. From the fit of the data to some model function one can obtain water permeability (Farinas et al. 1995). The main difference between the various techniques is how cell volume change as a function of time is measured. The experiments made up to now were performed on layers of kidney cells or on tissues and use light interference, fluorescence and other optical techniques where assumptions about the shape of the cells have to be done in order to obtain the variation of cell volume (Farinas et al. 1995, 1997, Timbs and Spring 1996, Zelenina and Brismar 2000, Maric et al. 2001).

One of the greatest difficulties in measuring water transport through cells is an accurate measurement of cell volume and volume variations. When cells adhere to a substrate they change their shape. Then, from 2D-images it is impossible to obtain an accurate value for cell volume. To circumvent such problem, with an optical tweezers, we hold a single MDCK kidney cell suspended in the solution medium, without touching the substrate or other cells. The single MDCK cell stays reasonably rounded such that its volume can be obtained from the video-image. We then, add to the external medium NaCl provoking a hyperosmotic shock. Water starts to leave the cell, and the volume decreases as can be seen in Figs. 7a, b.

A plot of normalized volume as a function of time is shown in Fig. 8.

After a while, the cell inflates again because of the increase in NaCl content inside the cell due to the slow flow through the semi-permeable biological membrane, and possibly also due to inner-cell electrolytes that flow into the osmotically active volume of the cell. In ref. (Lúcio et al. 2003) we made a simple phenomenological model to consider both the water transport and NaCl increase inside the cell, such that the data could be reasonably well described by this model. From our model we predict that the cell volume V as a function of time t varies as,

$$V(t) = Ae^{-\frac{t}{\tau_1}} - Be^{-\frac{t}{\tau_2}} + V_R, \qquad (4)$$

where A and B are constants related to water and NaCl permeabilities and osmotic shock load, τ_1 is a characteristic time for water transport, τ_2 a characteristic time for NaCl increase, and V_R is what we called the regulation volume, which is the new equilibrium volume after the osmotic shock. In ref. (Lúcio et al. 2003) it is shown how to relate τ_1, τ_2, A and B from Eq. 4 to the water permeability P, to electrolyte influx α, to the osmotically inactive volume b and to the initial volume V_0.

In Fig. 9 we show the results when one adds the antidiuretic hormone vasopressin. Water transport is faster and V_R decreases. Water transport is mediated by water channels (aquaporins) embedded in the cell surface membrane. Vasopressin increases their number on the surface of the cell increasing water permeability. Recently, Ateshian et al. (2006) made a more thermodynamically consistent model. They only consider passive loading of NaCl, *i.e.*, the NaCl increase inside the cell is only due to transport of NaCl from the external medium trough the semi-permeable cell membrane. In

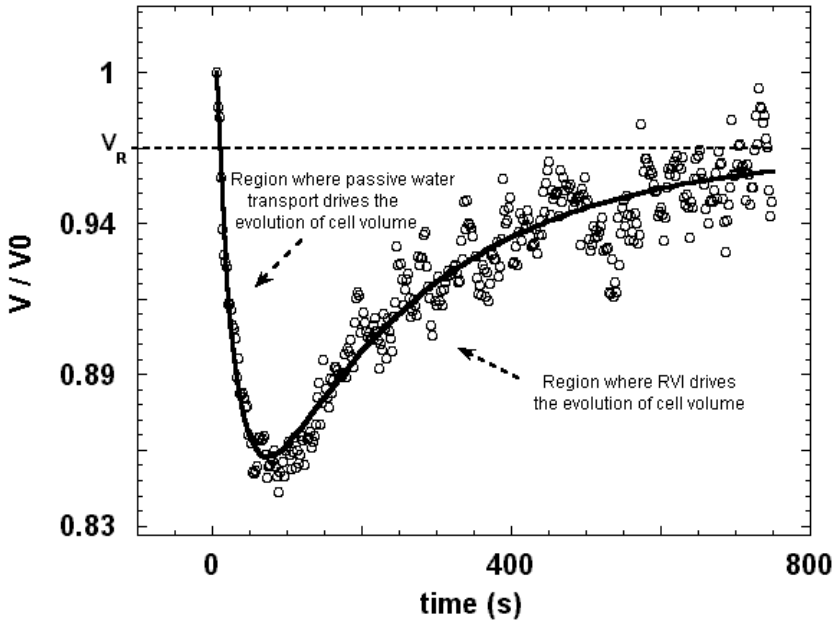

Fig. 8 – Time evolution of the normalized volume of the single MDCK cell of Figure 7, under osmotic up-shock from 300 mOsm to 500 mOsm. Circles are the experimental points and continuous curve is the fit using Equation 4. The fit returns $P = 6.6 \pm 0.3 \mu m/s$, $\alpha = (8.5 \pm 0.4)$ x $10^{-10} mol/s.cm^2$, $V_R/V_0 = 0.95 \pm 0.04$ and $b/V_0 = 0.52 \pm 0.02$.

this model V_R is determined by the equilibrium NaCl partition coefficient, which is the ratio of equilibrium NaCl concentration in the cytoplasm and the concentration in the medium. Their model involves nonlinear differential equations that can only be solved numerically. Our data of Fig. 9 was used in their article in support of their model. Why vasopressin changes the NaCl partition coefficient is yet to be explained.

MACROPHAGE MOTILITY AND PHAGOCYTOSIS

We are interested on how changes in macrophage cytoskeleton mechanical properties and motility can affect its phagocytic capacity. With the use of defocusing microscopy we are able to visualize the spreading plasma membrane of murine bone marrow macrophages adhered on glass slides, and make real-time observation and quantification of their membrane surface dynamics. Macrophage surface fluctuations are filmed with a CCD camera for posterior image analysis. Analysis of surface fluctuations indicate two main types of fluctuations: large coherent structures (ruffles) that move on the surface with some speed and small random fluctuations that

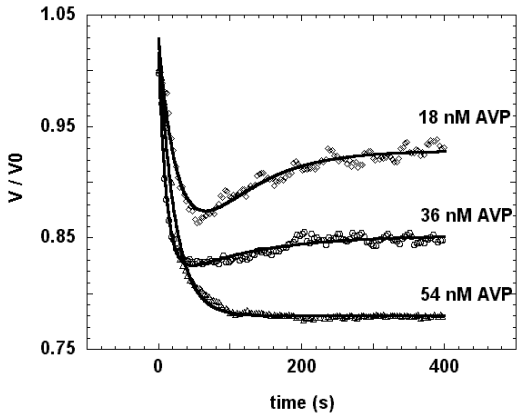

Fig. 9 – Time evolution of the normalized volume of trapped MDCK cells under an osmotic up-shock from 300 mOsm to 500 mOsm: lozenges are the data for vasopressin concentration of 18 nM, circles for 36 nM and triangles for 54 nM. Continuous curves are the fits using Eq. 4.

permeate the whole cell surface, as shown in Fig. 10.

We are able to measure height, width and speed of ruffles, time and spatial correlation functions and root

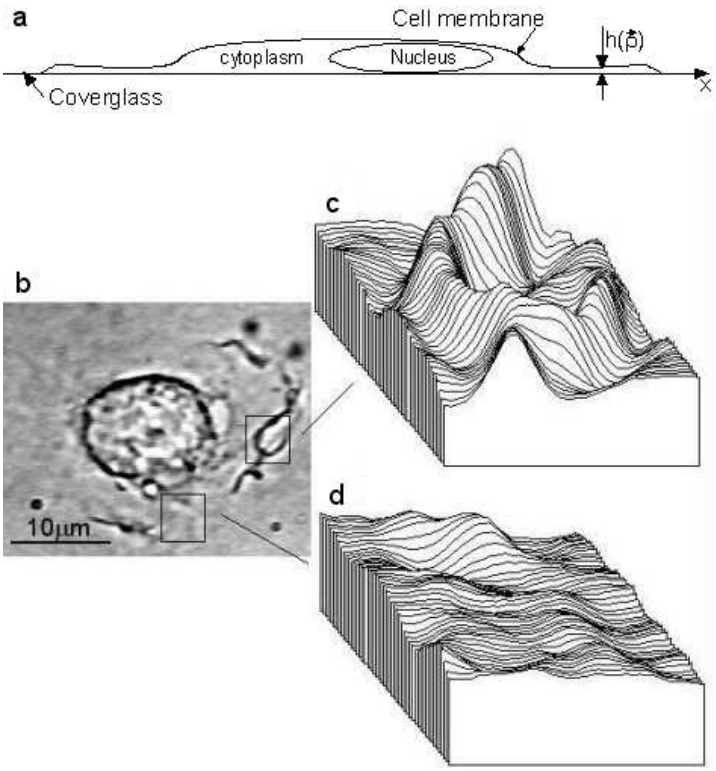

Fig. 10 – a) Sketch of a macrophage adhered on glass. b) Image of a macrophage obtained with microscope defocusing of $\Delta f = 1\mu m$. A movie of the macrophage 16.2 times faster can be seen at the site http://www.fisica.ufmg.br/ ∼estatexp/macrophage.mpg. c) Contrast profile (proportional to $\nabla^2 h(x, y)$) of kink-like structure propagating from the edge toward the nucleus of the cell. d) Contrast profile of small random fluctuations.

mean square values for curvature of the random fluctuations, either in presence of drugs or as a function of temperature. The elastic energy involved in these deformations is proportional to the square of curvature. Therefore, by measuring curvatures one can have one assessment of the energies involved to create small random fluctuations and ruffles. We estimate the energy to cause small random fluctuations and found it to be of the order of the thermal energy for T = 37°C. On the other hand to form a ruffle the energy cost is of the order of 100 times the thermal energy. Therefore, non-thermal energy is required to form ruffles. One can do a statistical analysis of the small random fluctuations by determining the time and spatial correlation functions of contrast fluctuations, which are related to cell surface curvature fluctuations. In Fig. 11 is shown time and spatial correlation functions of contrast fluctuations.

Performing this analysis on about 30 different macrophages we obtain a relaxation time of $\tau = 6 \pm 2$ s and a correlation length of $\xi = 0.24 \pm 0.02$ μm. From these results we obtain that the average amplitude of the small fluctuations is of the order of 3 nm, which is coincidentally, the size of actin subunits that form actin filaments, the bending modulus ($\sim 3.2 \times 10^{-19}$ J) and viscosity ($\sim$ 460 Pa.s) for the composite system membrane-plus-cytoskeleton. It seems then that the plasmatic membrane can fluctuate and make room for the addition of actin subunits into filaments that press the membrane. After some time the membrane can relax back by the removal of actin subunits. This picture is consistent with Brownian ratchet models of cytoskeleton motility (Peskin et al. 1993, Mogilner and Oster 1996). In a most recent model (Gov and Gopinathan 2006), surface proteins that trigger actin polymerization have been in-

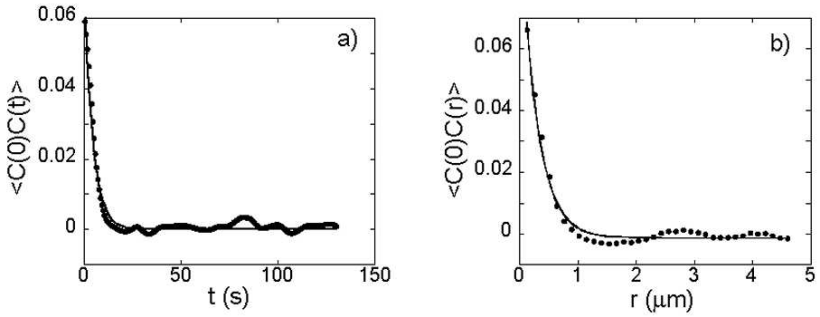

Fig. 11 – a) Temporal contrast autocorrelation function of random fluctuations with relaxation time $t = 4.5s$. b) Spatial contrast correlation function of random fluctuations with correlation length $\xi = 0.26\mu m$, which corresponds to the optical resolution of our microscope, indicating that the fluctuations are confined to regions with linear dimensions smaller than that.

corporated into the model and cause cell surface fluctuations and motility. The model predicts small height and curvature fluctuations, as well as ruffles, depending upon local protein concentrations. Our recent data (Coelho Neto et al. 2005) have been used by Gov and Gopinathan (Gov and Gopinathan 2006) in support of their model. We have also tried to correlate macrophage surface activity and phagocytic capacity. With the optical tweezers we grab a single Leishmania Amazonensis amastigote parasite and put it in contact with the membrane of a macrophage. As the macrophage starts to phagocyte the parasite, the optical tweezers is turned-off. This allows single phagocytosis events to be recorded and analyzed using defocusing microscopy. Our results indicate that in most of the events ($\sim$ 80%) the parasite can induce macrophage cell activity, by producing local ruffling around the phagocytic site. In this case the parasite is engulfed more rapidly than when there are no ruffling activity ($\sim$ 20% of the events). Since Leishmania is an obligatory intracellular parasite that resides inside macrophage lysosomes, the increase in ruffling activity could be induced by the parasite as an attempt to accelerate engulfment and facilitate infection. Our results for surface fluctuations relaxation time, speed of ruffles and phagocytosis time as a function of temperature, indicate that the dependence of all three parameters follow an Arrhenius-plot with activation energy around 34 $k_B T$, indicating a strong correlation between cytoskeleton motility and phagocytic capacity (Coelho Neto et al. 2005).

CONCLUSIONS

Optical tweezers are important tools for manipulating small objects (molecules or cells) and a very sensitive force sensor working in the picoNewton range. It has been used to study mechanical properties of a variety of bio-molecules and cells. In this work we showed that it can be used to study DNA-drug interaction in solution. In particular, we studied the interaction of the drug Psolaren with DNA, used in treatments of many skin diseases, since this interaction changes the entropic elasticity of DNA. With optical tweezers we are able to grab and suspend a single kidney cell in its medium and are able to measure its volume and volume variations during osmotic shocks to obtain important parameters related to osmotic transport through cell membrane.

Recently we introduced a new light microscopy technique that we named “defocusing microscopy” (DM), for visualization of transparent objects. The image contrast is proportional to the defocused distance and to the curvature of the object. We demonstrate that DM is able to provide quantitative data on macrophage surface motility and phagocytosis. We believe that it can be applied to many different cells for visualization and study of their mechanical properties. The wealth of data obtained is useful both to cell biologists and physicists interested in modeling biological phenomena.

ACKNOWLEDGMENTS

We thank our colleagues N.B. Viana, U. Agero, J. Coelho Neto, A.D. Lúcio, L.G. Mesquita and R.T. Gazzinelli,

for sharing with us their results. This work was supported by the Brazilian agencies: Conselho Nacional de Desenvolvimento Científico e Tecnológico (CNPq), Fundação de Amparo à Pesquisa do Estado de Minas Gerais (FAPEMIG), Financiadora de Estudos e Projetos – Programa de Apoio a Núcleos de Excelência (FINEP-PRONEX), Instituto do Milênio de Nanotecnologia – Ministério da Ciência e Tecnologia (MCT). M.S.R. acknowledges support by Laboratório Nacional de Luz Síncroton (LNLS).

RESUMO

Apresentamos uma revisão de duas novas técnicas para estudar propriedades biofísicas de moléculas únicas e células únicas. Um laser incidindo em uma objetiva de microscópio de grande abertura numérica é capaz de aprisionar pequenas partículas dielétricas na região próxima ao foco. Este aparato é chamado de pinça óptica. Esta técnica tem a grande vantagem de permitir a manipulação de um objeto individual. Usamos a pinça óptica para medir a elasticidade entrópica de uma molécula única de DNA em sua interação com o fármaco Psoralen. A pinça óptica também é usada para segurar uma célula renal MDCK fora do substrato, permitindo medidas precisas do volume dessa célula única durante um choque osmótico. Este processo nos permite obter informações sobre a permeabilidade osmótica da membrana e o crescimento do volume regulatório. A microscopia de desfocalização é uma técnica recente inventada em nosso laboratório, que nos permite observar objetos transparentes simplesmente desfocalizando o microscópio de uma maneira controlada. Nosso modelo físico de um microscópio desfocalizado mostra que o contraste da imagem observado neste caso é proporcional à distância da desfocalização e à curvatura do objeto transparente. A microscopia de desfocalização é muito útil para estudar a motilidade e as propriedades mecânicas das células. Mostramos aqui a aplicação da microscopia de desfocalização em medidas de flutuações na superfície de macrófagos e sua influência na fagocitose.

Palavras-chave: pinça óptica, microscopia de desfocalização, moléculas únicas, macrófagos, transporte de água, motilidade celular.

REFERENCES

AGERO U, MONKEN CH, ROPERT C, GAZZINELLI RT AND MESQUITA ON. 2003. Cell surface fluctuations studied with defocusing microscopy. Phys Rev E 67: 051904.

AGERO U, MESQUITA LG, NEVES BRA, GAZZINELLI RT AND MESQUITA ON. 2004. Defocusing microscopy. Microscopy Res Tech 65: 159–165.

AGRE P. 2000. Aquaporin water channels in kidney. J Am Soc Nephrol Apr 11: 764–777.

ASHKIN A. 1970. Acceleration and trapping of particles by radiation pressure. Phys Rev Lett 24: 156–&.

ASHKIN A. 1992. Forces of a single-beam gradient laser trap on a dielectric sphere in the ray optics regime. Biophys J 61: 569–582.

ASHKIN A AND DZIEDZIC JM. 1987. Optical trapping and manipulation of viruses and bacteria. Science 235: 1517–1520.

ATESHIAN GA, LIKHITPANICHKUL N AND HUNG CT. 2006. A mixture theory analysis for passive transport and osmotic loading cells. J Biomech 39: 464–475.

COELHO NETO J, OLIVEIRA DCP, GAZZINELLI RT AND MESQUITA ON. 2005. Real-time measurements of membrane surface dynamics on macrophages and the phagocytosis of *Leishmania* parasites. Exp Cell Res 303: 207–217.

COVEN TR, MURPHY FP AND GILLEAUDEAU P. 1998. Trimethylpsoralen bath PUVA is a remittive treatment for psoriasis vulgaris – Evidence that epidermal immunocytes are direct therapeutic targets. Arch Dermatol 134: 1263–1268.

FARINAS J, SIMANEK V AND VERKMAN AS. 1995. Cell-volume measured by total internal-reflection microfluorimetry – application to water and solute transport in cells transfected with water channel homologs. Biophys J 68: 1613–1620.

FARINAS J, KNEEN M, MOORE M AND VERKMAN AS. 1997. Plasma membrane water permeability of cultured cells and epithelia measured by light microscopy with spatial filtering. J Gen Physiol 10: 283–296.

GOV NS AND GOPINATHAN A. 2006. Dynamics of membranes driven by actin polymerization. Biophys J 90: 454–469.

GRIER DG. 2003. A revolution in optical manipulation. Nature 424: 810–816.

LÚCIO AD, SANTOS RAS AND MESQUITA ON. 2003. Measurements and modeling of water transport and osmoregulation in a single kidney cell using optical tweezers and videomicroscopy. Phys Rev E 68: 041906.

MAIA NETO PA AND NUSSENZVEIG HM. 2000. Theory of optical tweezers. Europhys Lett 50: 702–708.

MARIC K, WIESNER B, LORENZ D, KLUSSMANN E AND ROSENTHAL W. 2001. Cell volume kinetics of adherent

epithelial cells measured by laser scanning reflection microscopy: Determination of water permeability changes of renal principal cells. Biophys J 80: 1783–1790.

MARKO JF AND SIGGIA ED. 1995. Stretching DNA. Macromolecules 28: 8759–8770.

MAZOLLI A, MAIA NETO PA AND NUSSENZVEIG HM. 2003. Theory of trapping forces in optical tweezers. Proc Royal Soc London A 459: 3021–3041.

MOGILNER A AND OSTER GF. 1996. Cell motility driven by actin polymerization. Biophys J 71: 3030–3045.

PESKIN CS, ODELL GM AND OSTER GF. 1993. Cellular motion and thermal fluctuations: The brownian ratchet. Biophys J 65: 316–324.

ROCHA MS, VIANA NB AND MESQUITA ON. 2004. DNA-psoralen interaction: A single molecule experiment. J Chem Phys 121: 9679–9683.

SVOBODA K AND BLOCK SM. 1994. Biological applications of optical forces. Annu Rev Biophys Biomol Struct 23: 247–285.

TIMBS MM AND SPRING KR. 1996. Hydraulic properties of MDCK cell epithelium. J Membrane Biol 153: 1–11.

TRAN D, KWOK YK AND GOH CL. 2001. A retrospective review of PUVA therapy at the National Skin Centre of Singapore. Photodermatol Photo 17: 164–167.

VERKMAN S AND MITRA AK. 2000. Structure and function of aquaporin water channels. Am J Physiol – Renal Physiol 278: F13–F28.

VIANA NB, FREIRE RTS AND MESQUITA ON. 2002. Dynamic light scattering from an optically trapped microsphere. Phys Rev E 65: 041921.

ZEIDEL ML. 1998. Recent advances in water transport. Seminars in Nephrology 18: 167–177.

ZELENINA M AND BRISMAR H. 2000. Osmotic water permeability measurements using confocal laser scanning microscopy. Eur Biophys J 29: 165–171.